








A Preponderance of Perpendicular Planets

Simon H. Albrecht¹ , Marcus L. Marcussen¹ , Joshua N. Winn² , Rebekah I. Dawson³ , and Emil Knudstrup¹ 

¹ Stellar Astrophysics Centre, Department of Physics and Astronomy, Aarhus University, Ny Munkegade 120, DK-8000 Aarhus C, Denmark; albrecht@phys.au.dk

² Department of Astrophysical Sciences, Peyton Hall, 4 Ivy Lane, Princeton, NJ 08544, USA

³ Department of Astronomy & Astrophysics, Center for Exoplanets and Habitable Worlds, The Pennsylvania State University, University Park, PA 16802, USA

Received 2021 May 12; revised 2021 June 25; accepted 2021 June 25; published 2021 July 16

Abstract

Observing the Rossiter–McLaughlin effect during a planetary transit allows the determination of the angle λ between the sky projections of the star’s spin axis and the planet’s orbital axis. Such observations have revealed a large population of well-aligned systems and a smaller population of misaligned systems, with values of λ ranging up to 180° . For a subset of 57 systems, we can now go beyond the sky projection and determine the 3D obliquity ψ by combining the Rossiter–McLaughlin data with constraints on the line-of-sight inclination of the spin axis. Here we show that the misaligned systems do not span the full range of obliquities; they show a preference for nearly perpendicular orbits ($\psi = 80^\circ\text{--}125^\circ$) that seems unlikely to be a statistical fluke. If confirmed by further observations, this pile-up of polar orbits is a clue about the unknown processes of obliquity excitation and evolution.

Unified Astronomy Thesaurus concepts: Exoplanet dynamics (490); Exoplanet tides (497); Stellar rotation (1629); Exoplanet astronomy (486); Planet hosting stars (1242)

1. Introduction

An interesting development in exoplanet science was the discovery that a star’s direction of rotation need not be aligned with the orbital motion of its planets (Hébrard et al. 2008; Winn et al. 2009; Queloz et al. 2010). This fact came to light through observations of the Rossiter–McLaughlin (RM) effect, a spectroscopic anomaly during planetary transits that depends on the degree of spin–orbit alignment (Triaud 2017).

An obstacle to the interpretation of these results is that the RM effect depends mainly on the angle λ between the *sky projections* of the rotational and orbital axes, but the physically important angle is the obliquity ψ measured between the axes in three dimensions. See Figure 1 for a diagram of the angles, and Fabrycky & Winn (2009) for more details on the geometry.

To determine ψ , observations of the RM effect must be supplemented with information about the inclination i of the star’s rotation axis with respect to the line of sight. For example, a measurement of the star’s projected rotation velocity $v \sin i$ can be combined with the expected value of the rotation velocity v based on the star’s mass and age to arrive at a constraint on $\sin i$ (Schlaufman 2010). Recently, Louden et al. (2021) helped to set expectations for the rotation velocities of stars with effective temperatures between 5900 and 6600 K by measuring the $v \sin i$ distribution of a randomly oriented sample of stars. In reviewing the RM data for such stars, we noticed that whenever λ exceeds 90° , the inclination tends to be quite low, indicating a nearly polar orbit as opposed to a retrograde orbit. This pattern, shown in Figure 2, made us wonder if the 3D obliquity distribution shows a concentration near 90° even though the projected obliquity distribution spans the full range from 0° to 180° .

There is a growing number of stars for which the inclination can be determined directly from the data, even without prior expectations for the rotation velocity. In this Letter, we collect and analyze all of these systems (Section 2), and show that the distribution of ψ does indeed have a peak near 90° (Section 3). We perform tests of the statistical significance of this pattern

(Section 4) and consider possible biases (Section 5). Finally, we speculate on possible physical explanations (Section 6).

2. Sample Selection

Our starting point was the online database [TEPCAT](#) (Southworth et al. 2011a), which includes a compilation of results from RM observations. To the 155 systems that were in this database on 2021 January 5, we added K2-290 (Hjorth et al. 2021) for a total of 156.

Our main method for determining the stellar inclination angle was to combine measurements of the star’s projected rotation velocity ($v \sin i$), radius (R), and rotation period (P_{rot}):

$$\sin i = \frac{v \sin i}{v} = \frac{P_{\text{rot}} v \sin i}{2\pi R}. \quad (1)$$

The limiting factor was knowledge of the rotation period. A literature search turned up 38 cases in which the rotation period had been determined through photometric monitoring. We also analyzed all the available light curves from the Kepler, K2, and TESS missions using the autocorrelation method (McQuillan et al. 2013), which led to rotation period measurements for 28 stars. Of these, 15 were in agreement with values reported in the literature, and 13 had not been reported previously. All together we had 51 stars with measured rotation periods.

In addition, there are a few stars for which the stellar inclination angle was determined using a different method. For HAT-P-7, we used the result from the asteroseismic method, based on the relative amplitudes of the members of rotationally split multiplets in the oscillation spectrum. For KELT-9, KELT-17, Kepler-13, MASCARA-4, and WASP-189, we used results from the gravity-darkening method, based on modeling the distortions to the transit light curve due to the star’s equator-to-pole intensity gradient. Table 2 in the [Appendix](#) gives all the data and citations to the literature.

This made for a total of 57 systems for which we could determine the 3D obliquity. Figure 3 displays the key properties of the sample. Throughout this figure (and the two

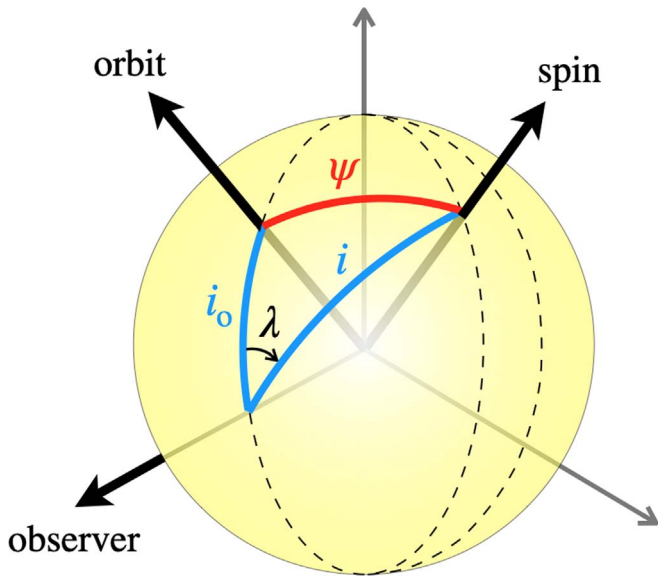


Figure 1. Geometry of the problem. Shown are the obliquity ψ , the sky-projected obliquity λ , the star’s inclination i , and the orbital inclination i_o (which is always near 90° for a transiting planet). Modeled after a similar figure by Perryman (2011).

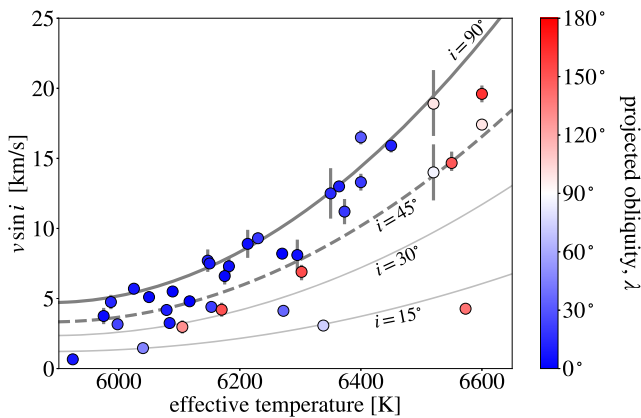


Figure 2. Suspectiously low $v \sin i$. Shown are all stars for which (i) λ has been measured, (ii) the effective temperature is within the plotted range, and (iii) the parameter $(m/M)(R/a)^3$ is less than 0.002, to avoid tidally spun-up stars. Whenever $\lambda > 90^\circ$ (white and red points), the $v \sin i$ is abnormally low. The thick line is the fitting function $v(T_{\text{eff}})$ from Louden et al. (2021), and the other lines are scaled for various inclinations. Of the eight stars with $\lambda > 90^\circ$, five (63%) have inclinations $< 45^\circ$, more than the 30% we would expect from a randomly oriented population.

figures to follow), the color of each data point conveys λ , with blue for 0° , white for 90° , and red for 180° . The upper left panel shows that the stars range from M dwarfs to A stars. The middle left plot shows $v \sin i$ versus effective temperature, including the sharp rise around 6250 K (the “Kraft break”). The lower left panel shows the subset of stars with measured rotation periods. The lower right panel shows rotation period as a function of main-sequence age, as estimated from stellar-evolutionary models. For reference, we highlighted the stars we expect to conform to the Skumanich law, $P_{\text{rot}} \propto \sqrt{t}$, indicated by the dashed line. Specifically, the highlighted stars have effective temperatures between 4000 and 6500 K and are unlikely to have been tidally spun up because $(m/M)(R/a)^3 > 0.002$ (corresponding to $a/R > 8$ for a Jupiter-mass planet around a Sun-like star).

3. Obliquity Distribution

For the stars with measured rotation periods, we used the method of Masuda & Winn (2020) to determine the posterior probability distribution for the obliquity, using the equation

$$\cos \psi = \sin i \sin i_o \cos \lambda + \cos i \cos i_o. \quad (2)$$

There are two solutions because the available observations cannot distinguish i from $180^\circ - i$, nor can they distinguish (i_o, λ) from $(180^\circ - i_o, -\lambda)$. The two solutions are closely spaced because $i_o \approx 90^\circ$.

In a few cases, the values of λ reported in the literature had uncertainties less than a degree. Out of concern about systematic errors, we imposed a minimum uncertainty of 1° in our analysis. For the same reason, we imposed a minimum uncertainty of 0.1 km s^{-1} in $v \sin i$. In all cases for which ψ had been reported previously in the literature, our results were in agreement. In four of these cases—HAT-P-11, K2-290, Kepler-63, and WASP-107—we adopted the previously reported value because it was based on more data.

Figure 4 shows the results as function of effective temperature. For ease of visual interpretation, instead of showing both solutions for ψ , we show the results assuming $i_o = 90^\circ$.⁴ The left panel of Figure 4 shows the distribution of λ , which ranges from 0° to 180° . The middle panel shows the distribution of ψ , in which there are two groups: 38 well-aligned systems with $\psi \lesssim 35^\circ$ and 18 systems with ψ in between 80° and 125° . The right panel shows the distribution of $\cos \psi$, which is easier to interpret visually because randomly oriented stars would have a uniform distribution in $\cos \psi$. As a less exact and more visual representation of the results, Figure 5 shows a 3D representation of the stellar spin orientations.

Seeking clues to the origin of this pattern, we tried to find something else the misaligned stars all have in common. Nothing stood out (see Figure 6). The misaligned group includes stars of spectral types A through M, orbital distances from 3 to 40 stellar radii, and planet masses from 0.1 to $3 M_{\text{Jup}}$. The three Neptune-mass planets GJ 436, HAT-P-11, and WASP-107 all have perpendicular orbits, as do the six hot Jupiters HAT-P-7, KELT-9, and WASP-7/76/189. The subgroup of systems with $\psi \approx 110^\circ$ consists of hot Jupiters around A, F, and G stars as well as the two-transiting-planet system K2-290. The lone star in between the aligned and misaligned groups is Kepler-13, with $\psi = 60^\circ$. This star also has the most massive planet among the misaligned stars ($4.9\text{--}8.1 M_{\text{Jup}}$; Shporer et al. 2014). This could be a coincidence, although it does conform to the previously noted pattern that the stars with the most massive planets are rarely found to have $\lambda > 90^\circ$ (Hébrard et al. 2011a).

4. Statistical Tests

We performed several statistical tests of the “null hypothesis” that the misaligned stars are randomly oriented instead of being clustered around $\psi \approx 90^\circ$. Defining misaligned stars as having $\cos \psi < 0.75$ ($\psi > 41^\circ$), the null hypothesis would lead to the expectation that $\cos \psi$ is uniformly distributed between -1 and 0.75 .

⁴ The median spacing between the two degenerate solutions is 0.2σ where σ is the statistical uncertainty, and the maximum spacing is 2σ .

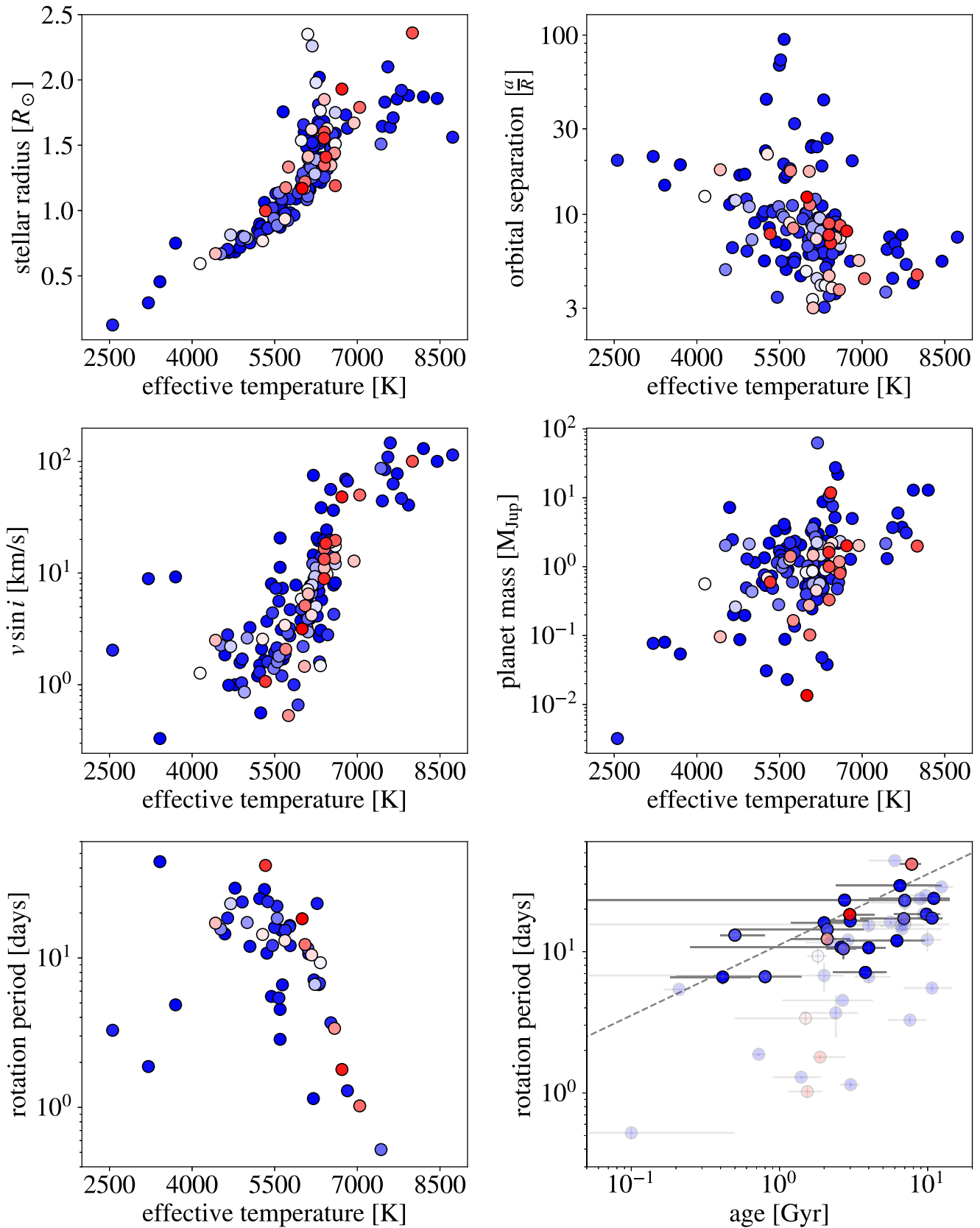


Figure 3. Stars with measurements of sky-projected obliquity. The color scale indicates λ , from blue for 0° to red for 180° . As a function of the star’s effective temperature, the left column shows the star’s radius (top), sky-projected rotation velocity (middle), and rotation period when available (bottom). The right column shows the planet’s orbital separation in units of the stellar radius (top) and mass (middle). The lower right panel shows the star’s rotation period versus age, with a line indicating the Skumanich law $P \propto \sqrt{t}$. The darker data points for which the stars are expected to obey the Skumanich law: $T_{\text{eff}} = 4500\text{--}6000$ K, $(m/M)(R/a)^3 < 0.002$.

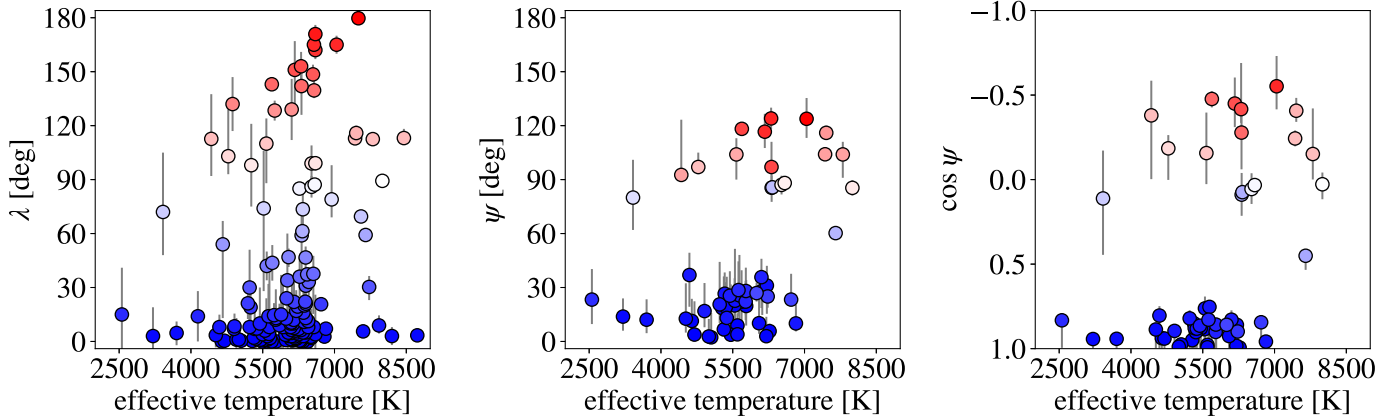


Figure 4. Obliquity distribution. Shown as a function of the star’s effective temperature are the sky-projected obliquity (left), the 3D obliquity (middle), and the cosine of the 3D obliquity (right).

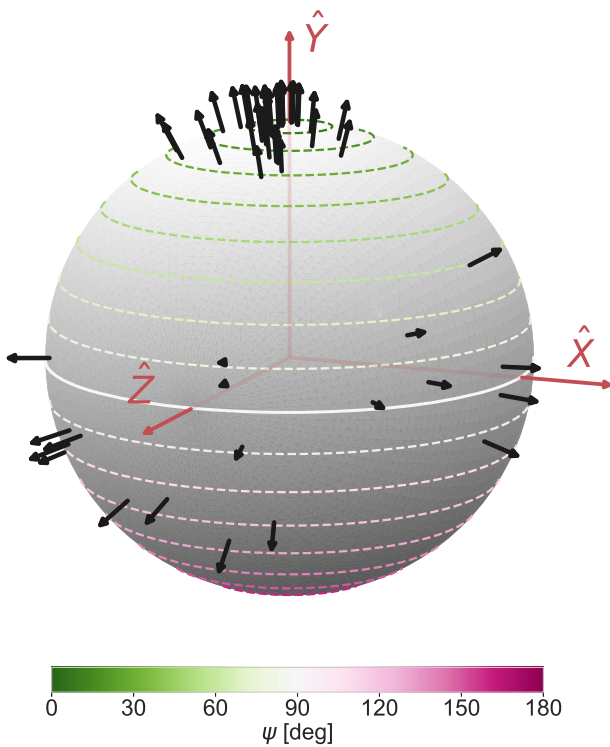


Figure 5. Obliquity distribution in 3D. The z -axis is the line of sight, and the y -axis is the orbital axis. The arrows represent the orientations of the stellar spin axes in our sample, and the colors of the latitudinal lines convey the obliquity. For plotting purposes, we broke the two-way degeneracy by choosing i and i_o to be $\leq 90^\circ$ and taking the signed value of λ from the literature.

One way to characterize the distribution of the misaligned stars is by the observed dispersion of $\cos \psi$ around zero:

$$\sigma_0 \equiv \sqrt{\frac{1}{N} \sum_{i=1}^N (\cos \psi_i)^2}, \quad (3)$$

where $N=19$. If $\cos \psi$ were distributed uniformly for the misaligned stars, how often would σ_0 be at least as small as is observed? To construct the expected distribution of σ_0 under this null hypothesis, we repeatedly drew 19 numbers from a uniform random distribution between -1 and 0.75 and calculated σ_0 in each case. Then, in each of 10^5 trials, we constructed a realization of the data by (i) choosing one of the

two solutions of Equation (2) at random for each data point, (ii) drawing a value of $\cos \psi$ from the observational posterior. For each realization of the data, we calculated the p -value of the null hypothesis. The median p -value was 3.1×10^{-3} .

We obtained similar results when replacing σ_0 by the standard deviation, i.e., when testing for clustering of $\cos \psi$ around the mean value, rather than around zero. Through similar Monte Carlo simulations, we found that the median p -value in that case is 9.6×10^{-4} .

The left column of Table 2 in the Appendix summarizes the results of these tests. While the p -values are low enough to reject the null hypothesis according to customary criteria, we acknowledge that the choices of the specific tests and the threshold value of $\cos \psi$ to qualify as “misaligned” were devised after seeing the data. As always in such cases, caution is warranted, and there is no substitute for getting additional data.

5. Possible Biases

The basic result of our study is that $|\cos \psi|$ tends to be small for the misaligned systems. Suppose that systematic errors in our input data have caused the inferred value of $|\cos \psi|$ to be biased by a factor f , i.e., when we infer $\cos \psi = x$ the true value is $x(1+f)$. How large would f need to be for the evidence for clustering around 90° to go away? We answered this question through another Monte Carlo simulation: we searched for the value of f that causes the median p -value to rise to 0.05 in the standard-deviation test described in the previous section. The answer is $f \approx 0.30$.

It seems unlikely that the inputs are biased at the 30% level. For the rotation period method, the obliquity is determined via the equation

$$\cos \psi \approx \cos \lambda \frac{P_{\text{rot}} v \sin i}{2\pi R}. \quad (4)$$

Therefore, a bias toward low $|\cos \psi|$ could be caused by:

1. Underestimating $v \sin i$. We adopted the results from analyses of RM data. Cross-checks with results based on spectral-line broadening indicate agreement within 10% with no discernible bias.
2. Overestimating R . The evolutionary models used to determine R are not perfect, but for these well-characterized stars any bias is likely to be $\lesssim 10\%$.

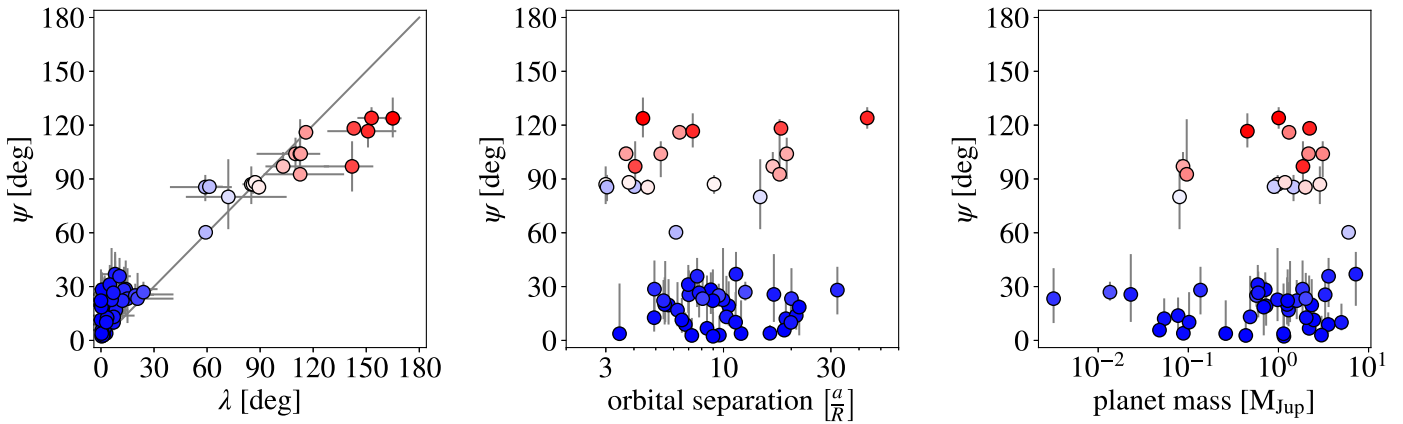


Figure 6. No trends seen. The 3D obliquity is plotted as a function of the sky-projected obliquity (left), the planet’s orbital separation (middle), and the planet’s mass (right).

Table 1
p-values

Test	Including Hottest Stars	Excluding Hottest Stars
Disp. around 90°	0.00310	0.0100
Disp. around mean	0.00096	0.0044

- Underestimating P_{rot} . Differential rotation probably introduces biases at the $\lesssim 10\%$ level. For example, the photometric period might be associated with features at different latitudes than those that contribute to the determination of $v \sin i$.

Another possible problem is that sometimes a photometric period is not the rotation period, but rather one-half of the rotation period, because spots occur on opposite hemispheres. Supposing this factor of 2 error occurred for n stars out of the sample of 19, we found through Monte Carlo simulation that we would need $n \gtrsim 6$ to cause the p -value of the standard-deviation test to rise to 0.05. We cannot exclude this possibility, though it seems doubtful given the good agreement between the periods we derived and the periods reported in the literature based on earlier data. Also, in many cases the measured rotation period conforms with expectations given the star’s mass and age (lower panels of Figure 3).

We also tried omitting the stars with $T_{\text{eff}} > 7000$ K from our statistical tests, for two reasons. First, for such hot stars, the photometric period might actually be a pulsation period instead of the rotation period. Second, our sample might be biased against hot stars with $\psi = 0^\circ$ or 180° because such stars would have larger $v \sin i$ values, making it more difficult to perform Doppler spectroscopy and confirm a planetary signal. The resulting p values, given in the second column of Table 1, are $\lesssim 0.01$.

6. Discussion

The literature contains a previous observational hint that nearly polar orbits are common, as well as several theoretical scenarios that might be relevant. On the observational side, Mazeh et al. (2015) found statistical evidence that stars with effective temperatures between about 6000 and 6500 K have high obliquities, with a possible preference for polar orbits.

This tentative conclusion was based on the observation that the amplitude of photometric variations associated with rotation was lower for stars with transiting planets than for randomly oriented stars. The correspondence with our sample is not exact, though: our stars span a wider range of effective temperatures, and our planets are generally larger than those analyzed by Mazeh et al. (2015).

On the theoretical side, four scenarios that could lead to obliquities near 90° are as follows:

- Tidal dissipation is usually thought to damp obliquities to 0° but in some cases can cause the obliquity to linger at 90° . Lai 2012 showed this can happen when the damping is dominated by the dissipation of inertial waves driven in the convective zone by Coriolis forces (see also Rogers & Lin 2013; Anderson et al. 2021). This theory might account for a few near-perpendicular systems. However, many systems have properties that seem incompatible with this theory: six have stars that lack convective zones ($T_{\text{eff}} > 7000$ K) and seven have orbital separations beyond 10 stellar radii where tides are expected to be negligible. Furthermore, 12 systems do not satisfy the criterion $P_{\text{rot}} > 2P_{\text{orb}}$ necessary to prevent tidal orbital decay, and 5 have large angular momentum ratios $L_{\text{orb}}/L_{\text{spin}}$ which would cause the obliquity to stall at 180° instead of 90° .
- Von Zeipel–Kozai–Lidov cycles, often invoked to explain hot Jupiters as the outcome of high-eccentricity tidal migration, were predicted to lead an obliquity distribution with a peak near 115° (Fabrycky & Tremaine 2007), a good match to the data. The predicted distribution also has a peak near 35° , while the low-obliquity group in our sample has $\langle \psi \rangle = 15^\circ$. Subsequent studies have shown that the predicted obliquity distribution depends on the orbital parameters of the perturber (Naoz et al. 2011), and the star’s mass and rotational oblateness and the planet’s mass (Anderson et al. 2016; Vick et al. 2019). It is worth revisiting these calculations to see if a better match to the data can be obtained. A scenario we are investigating is when the eccentricity required for high-eccentricity migration can only be induced by an outer companion on a nearly polar orbit; if the Jupiter begins its tidal migration near the general-relativistic quenching limit, the final obliquity would be near 90° .
- Secular resonance crossing was proposed by Petrovich et al. (2020) to explain the previously reported nearly

polar orbits of the Neptune-mass planets in our sample. The resonance between the disk-driven nodal precession frequencies of the transiting planet and an outer companion occurs as the disk decreases in mass. The resonance excites the inclination of the inner planet, and if the general relativistic precession rate is fast enough, the inclination is pushed up to 90° . Like the Von Zeipel–Kozai–Lidov scenario, the clearest prediction is that the nearly polar systems have massive outer companions. Petrovich et al. 2020 determined that the secular resonance crossing mechanism is most effective for lower-mass, close-orbiting planets, and low-mass, slowly rotating stars. Therefore, it is not clear that this mechanism would work for many of the systems in our sample.

4. Magnetic warping can tilt the young protoplanetary disk toward a perpendicular orientation, but other mechanisms can counteract this effect (e.g., accretion, magnetic braking, disk winds, differential precession, and wrapping of magnetic fields around the stellar rotational axis; Foucart & Lai 2011; Lai et al. 2011; Romanova et al. 2021).

Of course, nature is under no obligation to use only a single mechanism to tilt orbits and stars. We may find that the systems

in our sample have followed different paths to their nearly perpendicular configurations.

We thank R. Rubenzahl for providing posterior samples for λ and ψ based on his group’s analysis of WASP-107. J.N.W. thanks Cassandra Anderson and Scott Tremaine for interesting discussions. Funding for the Stellar Astrophysics Centre is provided by The Danish National Research Foundation (grant agreement No. DNRF106). Work by J.N.W. was partly supported by the Heising-Simons Foundation. R.I.D. is supported in part by NASA XRP NNX16AB50G. This paper includes data collected by the TESS mission, which was funded by the NASA Science Mission directorate. This research has made use of the [NASA Exoplanet Archive](#), which is operated by the California Institute of Technology, under contract with the National Aeronautics and Space Administration under the Exoplanet Exploration Program.

Facility: TESS.

Software: Matplotlib (Hunter 2007), astropy (Astropy Collaboration et al. 2013, 2018), spotify.

Appendix

Table 2 in this Appendix displays data used in this project. This also includes obliquity, ψ , values obtained as part of this work, as well as literature values.


Table 2
Listing of the Systems and Some Parameters

System	T_{eff} (K)	R (R_{\odot})	P_{rot} (days)	$v \sin i$ (km s^{-1})	λ ($^\circ$)	ψ ($^\circ$)	References
(1)	(2)	(3)	(4)	(5)	(6)	(7)	(8)
AU Mic	3700 ± 100	0.75 ± 0.03	4.85 ± 0.75	$9.23^{+0.79}_{-0.31}$	$4.7^{+6.4}_{-6.8}$	$12.1^{+11.3}_{-7.5}$	1
CoRoT-2	5598 ± 50	0.90 ± 0.02	4.52 ± 0.02	11.25 ± 0.45	$1.0^{+7.7}_{-6.0}$	$8.9^{+6.7}_{-5.1}$	2, 3
CoRoT-18	5440 ± 100	$0.88^{+0.03}_{-0.03}$	5.53 ± 0.33	8.00 ± 1.00	10.0 ± 20.0	$25.4^{+13.6}_{-13.1}$	4
DS Tuc	5598^{+28}_{-59}	0.87 ± 0.03	2.85 ± 0.06	$20.58^{+0.31}_{-0.24}$	$2.9^{+0.9}_{-0.9}$	$4.0^{+4.6}_{-1.6}$	5
EPIC 246851721	6202^{+52}_{-50}	$1.62^{+0.04}_{-0.04}$	1.14 ± 0.06	$74.92^{+0.62}_{-0.60}$	1.5 ± 0.9	$2.9^{+10.8}_{-1.6}$	6
GJ 436	3416 ± 54	0.46 ± 0.02	44.09 ± 0.08	$0.33^{+0.09}_{-0.07}$	$72.0^{+33.0}_{-24.0}$	$80.0^{+21.0}_{-18.0}$	7
HAT-P-7	6310 ± 15	2.02 ± 0.01	...	2.70 ± 0.50	$142.0^{+12.0}_{-16.0}$	97.0 ± 14.0	8, 9, 10
HAT-P-11	4780 ± 50	0.68 ± 0.01	29.32 ± 1.00	$1.00^{+0.95}_{-0.56}$	$103.0^{+26.0}_{-10.0}$	$97.0^{+8.0}_{-4.0}$	11, 12, 13
HAT-P-20	4595 ± 45	0.68 ± 0.01	14.48 ± 0.02	1.85 ± 0.27	8.0 ± 6.9	$36.9^{+12.4}_{-17.6}$	14
HAT-P-22	5314 ± 50	1.06 ± 0.05	28.70 ± 0.40	1.65 ± 0.26	2.1 ± 3.0	$6.7^{+29.4}_{-3.8}$	15
HAT-P-36	5620 ± 40	1.04 ± 0.02	15.30 ± 0.40	3.12 ± 0.75	14.0 ± 18.0	$28.6^{+16.0}_{-14.6}$	16
HATS-2	5227 ± 95	0.90 ± 0.02	24.98 ± 0.04	1.50 ± 0.50	8.0 ± 8.0	$20.6^{+23.6}_{-10.4}$	2, 17
HD 63433	5640 ± 74	$0.91^{+0.03}_{-0.03}$	6.61 ± 0.71	7.30 ± 0.30	$8.0^{+33.0}_{-45.0}$	$25.6^{+22.5}_{-15.3}$	18, 19
HD 189733	5050 ± 50	0.75 ± 0.03	11.95 ± 0.02	3.25 ± 0.02	0.4 ± 0.2	$2.3^{+13.5}_{-1.6}$	20, 21
HD 209458	6117 ± 50	1.16 ± 0.01	10.65 ± 0.75	4.80 ± 0.20	0.6 ± 0.4	$28.2^{+9.7}_{-13.5}$	22, 23
K2-25	3207 ± 58	0.29 ± 0.01	1.88 ± 0.04	8.90 ± 0.60	3.0 ± 16.0	$13.8^{+10.1}_{-7.8}$	24
K2-29	5358 ± 38	0.86 ± 0.01	10.76 ± 0.22	3.70 ± 0.50	1.5 ± 8.7	$19.3^{+13.7}_{-11.1}$	25
K2-290	6302 ± 120	$1.51^{+0.08}_{-0.08}$	6.63 ± 0.66	$6.90^{+0.50}_{-0.60}$	153.0 ± 8.0	124.0 ± 6.0	26, 27
KELT-9	9600 ± 400	2.42 ± 0.06	...	116.90 ± 1.80	85.0 ± 0.2	$87.0^{+10.0}_{-11.0}$	28, 29
KELT-17	7454 ± 49	$1.65^{+0.06}_{-0.06}$...	$44.20^{+1.50}_{-1.30}$	115.9 ± 4.1	116.0 ± 4.0	30
Kepler-8	6213 ± 150	1.50 ± 0.04	7.13 ± 0.14	8.90 ± 1.00	5.0 ± 7.0	$31.1^{+10.9}_{-15.7}$	8
Kepler-9	5774 ± 60	0.96 ± 0.02	16.49 ± 0.33	2.74 ± 0.40	13.0 ± 16.0	$28.1^{+13.0}_{-13.6}$	31
Kepler-13	7650 ± 250	1.71 ± 0.04	...	62.70 ± 0.20	59.2 ± 0.1	60.2 ± 0.1	32
Kepler-17	5781 ± 85	$0.98^{+0.02}_{-0.05}$	12.09 ± 0.24	4.70 ± 1.00	0.0 ± 15.0	$19.7^{+14.4}_{-10.9}$	33
Kepler-25	6270 ± 79	$1.32^{+0.02}_{-0.01}$	23.15 ± 0.04	8.20 ± 0.20	0.5 ± 5.7	$5.7^{+4.2}_{-3.2}$	34, 35
Kepler-63	5576 ± 50	$0.90^{+0.03}_{-0.02}$	5.40 ± 0.01	5.60 ± 0.80	$110.0^{+14.0}_{-22.0}$	$104.0^{+9.0}_{-14.0}$	22, 36
Kepler-448	6820 ± 120	1.63 ± 0.15	1.29 ± 0.03	$66.43^{+1.00}_{-0.95}$	$7.1^{+2.8}_{-4.2}$	$10.0^{+10.4}_{-4.5}$	37
MASCARA-4	7800 ± 200	1.92 ± 0.11	...	46.50 ± 1.00	$112.5^{+1.7}_{-1.5}$	$104.0^{+7.0}_{-13.0}$	38, 39
Qatar-1	4910 ± 100	0.80 ± 0.02	23.70 ± 0.12	1.70 ± 0.30	8.4 ± 7.1	$16.9^{+5.6}_{-9.0}$	40, 41
Qatar-2	4645 ± 50	0.70 ± 0.01	18.50 ± 1.90	2.80 ± 0.50	0.0 ± 8.0	$11.4^{+12.3}_{-7.1}$	42, 43, 44

Table 2
(Continued)

System	T_{eff} (K)	R (R_{\odot})	P_{rot} (days)	$v \sin i$ (km s^{-1})	λ ($^{\circ}$)	ψ ($^{\circ}$)	References
(1)	(2)	(3)	(4)	(5)	(6)	(7)	(8)
TRAPPIST-1	2557 ± 47	0.12 ± 0.00	3.28 ± 0.22	2.04 ± 0.18	$15.0^{+26.0}_{-30.0}$	$23.3^{+17.0}_{-13.6}$	45
WASP-4	5540 ± 55	0.91 ± 0.02	22.20 ± 3.30	$2.14^{+0.38}_{-0.35}$	$1.0^{+12.0}_{-14.0}$	$20.0^{+15.2}_{-11.1}$	2, 46
WASP-5	5770 ± 65	1.09 ± 0.04	16.20 ± 0.40	3.20 ± 0.30	$12.1^{+8.0}_{-10.0}$	$22.2^{+11.5}_{-10.3}$	2, 47
WASP-6	5375 ± 65	0.86 ± 0.03	23.80 ± 0.15	$1.60^{+0.27}_{-0.17}$	7.2 ± 3.7	$13.1^{+22.9}_{-3.8}$	2, 48, 49
WASP-7	6520 ± 70	1.48 ± 0.09	3.68 ± 1.23	14.00 ± 2.00	86.0 ± 6.0	$87.1^{+5.1}_{-5.3}$	50
WASP-8	5690 ± 36	0.98 ± 0.02	15.31 ± 0.80	1.90 ± 0.05	$143.0^{+1.5}_{-1.6}$	$118.2^{+3.2}_{-3.0}$	51
WASP-12	6313 ± 52	$1.66^{+0.05}_{-0.04}$	6.77 ± 1.58	$1.60^{+0.80}_{-0.40}$	$59.0^{+15.0}_{-20.0}$	$85.5^{+6.8}_{-7.8}$	8
WASP-19	5460 ± 90	1.02 ± 0.01	12.13 ± 2.10	4.40 ± 0.90	1.0 ± 1.2	$3.7^{+28.0}_{-2.3}$	8, 52
WASP-32	6100 ± 100	1.11 ± 0.05	11.60 ± 1.00	$3.90^{+0.40}_{-0.50}$	$10.5^{+6.4}_{-6.5}$	$35.8^{+10.2}_{-17.2}$	53, 54
WASP-33	7430 ± 100	$1.51^{+0.02}_{-0.03}$	0.52 ± 0.05	$86.63^{+0.32}_{-0.37}$	$112.9^{+0.2}_{-0.2}$	$104.1^{+2.8}_{-2.8}$	55
WASP-41	5546 ± 33	0.89 ± 0.01	18.41 ± 0.05	1.60 ± 1.10	6.0 ± 11.0	$22.6^{+28.9}_{-11.9}$	2, 56
WASP-43	4520 ± 120	$0.67^{+0.01}_{-0.01}$	15.60 ± 0.40	2.26 ± 0.54	3.5 ± 6.8	$12.7^{+19.7}_{-7.7}$	2, 14
WASP-52	5000 ± 100	0.79 ± 0.02	$17.26^{+0.51}_{-0.39}$	2.62 ± 0.07	1.1 ± 1.1	$2.8^{+9.8}_{-1.8}$	57, 58
WASP-62	6230 ± 80	1.28 ± 0.05	6.65 ± 0.13	9.30 ± 0.20	$19.4^{+5.1}_{-4.9}$	$25.0^{+6.6}_{-6.2}$	59
WASP-69	4700 ± 50	0.81 ± 0.03	23.07 ± 0.16	2.20 ± 0.40	$0.4^{+2.0}_{-1.9}$	$3.8^{+18.5}_{-2.7}$	2, 60
WASP-76	6329 ± 65	1.76 ± 0.07	9.29 ± 1.27	1.48 ± 0.28	$61.3^{+7.6}_{-5.1}$	$85.7^{+2.5}_{-2.4}$	61
WASP-84	5280 ± 80	0.77 ± 0.02	14.36 ± 0.35	2.56 ± 0.08	0.3 ± 1.7	$18.6^{+4.4}_{-15.7}$	2, 62
WASP-85	5685 ± 65	0.94 ± 0.02	13.08 ± 0.26	3.41 ± 0.89	0.0 ± 14.0	$22.1^{+17.4}_{-12.1}$	63
WASP-94A	6170 ± 80	$1.62^{+0.05}_{-0.04}$	10.48 ± 1.60	4.20 ± 0.50	$151.0^{+16.0}_{-23.0}$	$116.6^{+9.9}_{-9.1}$	64
WASP-107	4425 ± 70	0.67 ± 0.02	17.10 ± 1.00	2.50 ± 0.80	$112.6^{+24.9}_{-20.6}$	$92.6^{+30.7}_{-1.8}$	65, 66
WASP-121	6586 ± 59	1.44 ± 0.03	3.38 ± 0.40	$13.56^{+0.69}_{-0.68}$	$87.2^{+0.4}_{-0.4}$	88.1 ± 0.2	67
WASP-166	6050 ± 50	1.22 ± 0.06	12.30 ± 1.90	5.10 ± 0.30	3.0 ± 5.0	$10.1^{+16.7}_{-5.9}$	68
WASP-167	7043^{+89}_{-68}	1.79 ± 0.05	1.02 ± 0.10	49.94 ± 0.04	165.0 ± 5.0	$123.8^{+11.6}_{-10.6}$	69
WASP-189	8000 ± 80	2.36 ± 0.03	...	100.00 ± 5.00	89.3 ± 1.4	85.4 ± 4.3	70, 71
XO-2	5332 ± 57	$1.00^{+0.03}_{-0.03}$	41.60 ± 1.10	1.07 ± 0.09	7.0 ± 11.0	$26.5^{+11.8}_{-13.7}$	72
XO-6	6720 ± 100	1.93 ± 0.18	1.79 ± 0.06	48.00 ± 3.00	20.7 ± 2.3	$23.3^{+14.3}_{-2.9}$	73
pi Men	5998 ± 62	1.17 ± 0.02	18.30 ± 1.00	3.16 ± 0.27	24.0 ± 4.1	$26.9^{+5.8}_{-4.7}$	74, 75

Note. The quoted $1 - \sigma$ values for P_{rot} and ψ are obtained from the highest density regions. If not derived in this work then values are either taken from TRAPPIST (1) Hirano et al. (2020a), (2) Bonomo et al. (2017), (3) Czesla et al. (2012), (4) Hébrard et al. (2011b), (5) Zhou et al. (2020), (6) Yu et al. (2018), (7) Bourrier et al. (2018), (8) Albrecht et al. (2012b), (9) Masuda (2015), (10) Lund et al. (2014), (11) Béky et al. (2014), (12) Winn et al. (2010), (13) Sanchis-Ojeda & Winn (2011), (14) Esposito et al. (2017), (15) Mancini et al. (2018), (16) Mancini et al. (2015), (17) Mohler-Fischer et al. (2013), (18) Mann et al. (2020), (19) Dai et al. (2020), (20) Henry & Winn (2008), (21) Cegla et al. (2016), (22) Maxted et al. (2015), (23) Santos et al. (2020), (24) Stefansson et al. (2020), (25) Santerne et al. (2016), (26) Hjorth et al. (2019), (27) Hjorth et al. (2021), (28) Wyttenbach et al. (2020), (29) Ahlers et al. (2020a), (30) Zhou et al. (2016), (31) Wang et al. (2018), (32) Howarth & Morello (2017), (33) Désert et al. (2011), (34) McQuillan et al. (2013), (35) Albrecht et al. (2013), (36) Sanchis-Ojeda et al. (2013), (37) Johnson et al. (2017), (38) Dorval et al. (2020), (39) Ahlers et al. (2020b), (40) Mislis et al. (2015), (41) Covino et al. (2013), (42) Dai et al. (2017), (43) Bryan et al. (2012), (44) Močnik et al. (2017), (45) Hirano et al. (2020b), (46) Sanchis-Ojeda et al. (2011), (47) Triaud et al. (2010), (48) Gillon et al. (2009), (49) Tregloan-Reed et al. (2015), (50) Albrecht et al. (2012a), (51) Bourrier et al. (2017), (52) Tregloan-Reed et al. (2013), (53) Brothwell et al. (2014), (54) Brown et al. (2012), (55) Johnson et al. (2015), (56) Southworth et al. (2011b), (57) Rosich et al. (2020), (58) Chen et al. (2020), (59) Brown et al. (2017), (60) Casasayas-Barris et al. (2017), (61) Ehrenreich et al. (2020), (62) Anderson et al. (2015), (63) Močnik et al. (2016), (64) Neveu-VanMalle et al. (2014), (65) Anderson et al. (2017), (66) Rubenzahl et al. (2021), (67) Bourrier et al. (2020), (68) Hellier et al. (2019), (69) Temple et al. (2017), (70) Anderson et al. (2018), (71) Lendl et al. (2020), (72) Damasso et al. (2015), (73) Crouzet et al. (2017), (74) Zurlo et al. (2018), or (75) Kunovac Hodžić et al. (2021)

ORCID iDsSimon H. Albrecht  <https://orcid.org/0000-0003-1762-8235>Marcus L. Marcussen  <https://orcid.org/0000-0003-2173-0689>Joshua N. Winn  <https://orcid.org/0000-0002-4265-047X>Rebekah I. Dawson  <https://orcid.org/0000-0001-9677-1296>Emil Knudstrup  <https://orcid.org/0000-0001-7880-594X>**References**

Ahlers, J. P., Johnson, M. C., Stassun, K. G., et al. 2020a, *AJ*, 160, 4
 Ahlers, J. P., Kruse, E., Colón, K. D., et al. 2020b, *ApJ*, 888, 63
 Albrecht, S., Winn, J. N., Butler, R. P., et al. 2012a, *ApJ*, 744, 189
 Albrecht, S., Winn, J. N., Johnson, J. A., et al. 2012b, *ApJ*, 757, 18

Albrecht, S., Winn, J. N., Marcy, G. W., et al. 2013, *ApJ*, 771, 11
 Anderson, D. R., Collier Cameron, A., Delrez, L., et al. 2017, *A&A*, 604, A110
 Anderson, D. R., Temple, L. Y., Nielsen, L. D., et al. 2018, arXiv:1809.04897
 Anderson, D. R., Triaud, A. H. M. J., Turner, O. D., et al. 2015, *ApJL*, 800, L9
 Anderson, K. R., Storch, N. I., & Lai, D. 2016, *MNRAS*, 456, 3671
 Anderson, K. R., Winn, J. N., & Penev, K. 2021, *ApJ*, 914, 56
 Astropy Collaboration, Price-Whelan, A. M., Sipőcz, B. M., et al. 2018, *AJ*, 156, 123
 Astropy Collaboration, Robitaille, T. P., Tollerud, E. J., et al. 2013, *A&A*, 558, A33
 Béky, B., Holman, M. J., Kipping, D. M., & Noyes, R. W. 2014, *ApJ*, 788, 1
 Bonomo, A. S., Desidera, S., Benatti, S., et al. 2017, *A&A*, 602, A107
 Bourrier, V., Cegla, H. M., Lovis, C., & Wyttenbach, A. 2017, *A&A*, 599, A33
 Bourrier, V., Ehrenreich, D., Lendl, M., et al. 2020, *A&A*, 635, A205
 Bourrier, V., Lovis, C., Beust, H., et al. 2018, *Natur*, 553, 477
 Brothwell, R. D., Watson, C. A., Hébrard, G., et al. 2014, *MNRAS*, 440, 3392

- Brown, D. J. A., Collier Cameron, A., & Díaz, R. F. 2012, *ApJ*, 760, 139
- Brown, D. J. A., Triaud, A. H. M. J., Doyle, A. P., et al. 2017, *MNRAS*, 464, 810
- Bryan, M. L., Alsubai, K. A., Latham, D. W., et al. 2012, *ApJ*, 750, 84
- Casasayas-Barris, N., Palle, E., Nowak, G., et al. 2017, *A&A*, 608, A135
- Cegla, H. M., Lovis, C., Bourrier, V., et al. 2016, *A&A*, 588, A127
- Chen, G., Casasayas-Barris, N., Pallé, E., et al. 2020, *A&A*, 635, A171
- Covino, E., Esposito, M., Barbieri, M., et al. 2013, *A&A*, 554, A28
- Crouzet, N., McCullough, P. R., Long, D., et al. 2017, *AJ*, 153, 94
- Czesla, S., Schröter, S., Wolter, U., et al. 2012, *A&A*, 539, A150
- Dai, F., Roy, A., Fulton, B., et al. 2020, *AJ*, 160, 193
- Dai, F., Winn, J. N., Yu, L., & Albrecht, S. 2017, *AJ*, 153, 40
- Damasso, M., Biazzo, K., Bonomo, A. S., et al. 2015, *A&A*, 575, A111
- Désert, J.-M., Charbonneau, D., Demory, B.-O., et al. 2011, *ApJS*, 197, 14
- Dorval, P., Talens, G. J. J., Otten, G. P. L., et al. 2020, *A&A*, 635, A60
- Ehrenreich, D., Lovis, C., Allart, R., et al. 2020, *Natur*, 580, 597
- Esposito, M., Covino, E., Desidera, S., et al. 2017, *A&A*, 601, A53
- Fabrycky, D., & Tremaine, S. 2007, *ApJ*, 669, 1298
- Fabrycky, D. C., & Winn, J. N. 2009, *ApJ*, 696, 1230
- Foucart, F., & Lai, D. 2011, *MNRAS*, 412, 2799
- Gillon, M., Anderson, D. R., Triaud, A. H. M. J., et al. 2009, *A&A*, 501, 785
- Hébrard, G., Bouchy, F., Pont, F., et al. 2008, *A&A*, 488, 763
- Hébrard, G., Ehrenreich, D., Bouchy, F., et al. 2011a, *A&A*, 527, L11
- Hébrard, G., Evans, T. M., Alonso, R., et al. 2011b, *A&A*, 533, A130
- Hellier, C., Anderson, D. R., Triaud, A. H. M. J., et al. 2019, *MNRAS*, 488, 3067
- Henry, G. W., & Winn, J. N. 2008, *AJ*, 135, 68
- Hirano, T., Gaidos, E., Winn, J. N., et al. 2020b, *ApJL*, 890, L27
- Hirano, T., Krishnamurthy, V., Gaidos, E., et al. 2020a, *ApJL*, 899, L13
- Hjorth, M., Albrecht, S., Hirano, T., et al. 2021, *PNAS*, 118, 2017418118
- Hjorth, M., Justesen, A. B., Hirano, T., et al. 2019, *MNRAS*, 484, 3522
- Howarth, I. D., & Morello, G. 2017, *MNRAS*, 470, 932
- Hunter, J. D. 2007, *CSE*, 9, 90
- Johnson, M. C., Cochran, W. D., Addison, B. C., Tinney, C. G., & Wright, D. J. 2017, *AJ*, 154, 137
- Johnson, M. C., Cochran, W. D., Collier Cameron, A., & Bayliss, D. 2015, *ApJL*, 810, L23
- Kunovac Hodžić, V., Triaud, A. H. M. J., Cegla, H. M., Chaplin, W. J., & Davies, G. R. 2021, *MNRAS*, 502, 2893
- Lai, D. 2012, *MNRAS*, 423, 486
- Lai, D., Foucart, F., & Lin, D. N. C. 2011, *MNRAS*, 412, 2790
- Lendl, M., Csizmadia, S., Deline, A., et al. 2020, *A&A*, 643, A94
- Louden, E. M., Winn, J. N., Petigura, E. A., et al. 2021, *AJ*, 161, 68
- Lund, M. N., Lundkvist, M., Silva Aguirre, V., et al. 2014, *A&A*, 570, A54
- Mancini, L., Esposito, M., Covino, E., et al. 2015, *A&A*, 579, A136
- Mancini, L., Esposito, M., Covino, E., et al. 2018, *A&A*, 613, A41
- Mann, A. W., Johnson, M. C., Vanderburg, A., et al. 2020, *AJ*, 160, 179
- Masuda, K. 2015, *ApJ*, 805, 28
- Masuda, K., & Winn, J. N. 2020, *AJ*, 159, 81
- Maxted, P. F. L., Serenelli, A. M., & Southworth, J. 2015, *A&A*, 577, A90
- Mazeh, T., Perets, H. B., McQuillan, A., & Goldstein, E. S. 2015, *ApJ*, 801, 3
- McQuillan, A., Mazeh, T., & Aigrain, S. 2013, *ApJL*, 775, L11
- Mislis, D., Mancini, L., Tregloan-Reed, J., et al. 2015, *MNRAS*, 448, 2617
- Močnik, T., Clark, B. J. M., Anderson, D. R., Hellier, C., & Brown, D. J. A. 2016, *AJ*, 151, 150
- Močnik, T., Southworth, J., & Hellier, C. 2017, *MNRAS*, 471, 394
- Mohler-Fischer, M., Mancini, L., Hartman, J. D., et al. 2013, *A&A*, 558, A55
- Naoz, S., Farr, W. M., Lithwick, Y., Rasio, F. A., & Teyssandier, J. 2011, *Natur*, 473, 187
- Neveu-VanMalle, M., Queloz, D., Anderson, D. R., et al. 2014, *A&A*, 572, A49
- Perryman, M. 2011, *The Exoplanet Handbook* (Cambridge: Cambridge Univ. Press)
- Petrovich, C., Muñoz, D. J., Kratter, K. M., & Malhotra, R. 2020, *ApJL*, 902, L5
- Queloz, D., Anderson, D., Collier Cameron, A., et al. 2010, *A&A*, 517, L1
- Rogers, T. M., & Lin, D. N. C. 2013, *ApJL*, 769, L10
- Romanova, M. M., Koldoba, A. V., Ustyugova, G. V., et al. 2021, *MNRAS*, 506, 372
- Rosich, A., Herrero, E., Mallonn, M., et al. 2020, *A&A*, 641, A82
- Rubenzahl, R. A., Dai, F., Howard, A. W., et al. 2021, *AJ*, 161, 119
- Sanchis-Ojeda, R., & Winn, J. N. 2011, *ApJ*, 743, 61
- Sanchis-Ojeda, R., Winn, J. N., Holman, M. J., et al. 2011, *ApJ*, 733, 127
- Sanchis-Ojeda, R., Winn, J. N., Marcy, G. W., et al. 2013, *ApJ*, 775, 54
- Santerne, A., Hébrard, G., Lillo-Box, J., et al. 2016, *ApJ*, 824, 55
- Santos, N. C., Cristo, E., Demangeon, O., et al. 2020, *A&A*, 644, A51
- Schlaufman, K. C. 2010, *ApJ*, 719, 602
- Shporer, A., O'Rourke, J. G., Knutson, H. A., et al. 2014, *ApJ*, 788, 92
- Southworth, J., Dominik, M., Jørgensen, U. G., et al. 2011a, *A&A*, 527, A8
- Southworth, J., Tregloan-Reed, J., Andersen, M. I., et al. 2011b, *MNRAS*, 417, 2166
- Stefansson, G., Mahadevan, S., Maney, M., et al. 2020, *AJ*, 160, 192
- Temple, L. Y., Hellier, C., Albrow, M. D., et al. 2017, *MNRAS*, 471, 2743
- Tregloan-Reed, J., Southworth, J., Burgdorf, M., et al. 2015, *MNRAS*, 450, 1760
- Tregloan-Reed, J., Southworth, J., & Tappert, C. 2013, *MNRAS*, 428, 3671
- Triaud, A. H. M. J. 2017, in *Exoplanet Research*, ed. H. Deeg & J. Belmonte (Cham: Springer)
- Triaud, A. H. M. J., Collier Cameron, A., Queloz, D., et al. 2010, *A&A*, 524, A25
- Vick, M., Lai, D., & Anderson, K. R. 2019, *MNRAS*, 484, 5645
- Wang, S., Addison, B., Fischer, D. A., et al. 2018, *AJ*, 155, 70
- Winn, J. N., Johnson, J. A., Fabrycky, D., et al. 2009, *ApJ*, 700, 302
- Winn, J. N., Johnson, J. A., Howard, A. W., et al. 2010, *ApJL*, 723, L223
- Wytenbach, A., Mollière, P., Ehrenreich, D., et al. 2020, *A&A*, 638, A87
- Yu, L., Zhou, G., Rodriguez, J. E., et al. 2018, *AJ*, 156, 250
- Zhou, G., Rodriguez, J. E., Collins, K. A., et al. 2016, *AJ*, 152, 136
- Zhou, G., Winn, J. N., Newton, E. R., et al. 2020, *ApJL*, 892, L21
- Zurlo, A., Mesa, D., Desidera, S., et al. 2018, *MNRAS*, 480, 35